3D synthetic aperture for diffusive fields

Allison Knaak[1], Roel Snieder[1], Yuanzhong Fan[2], David Ramirez-Mejia[2], & Mark Rosenquist[2]

[1] *Center for Wave Phenomena, Colorado School of Mines, Golden, CO 80401, USA*
[2] *Shell International Exploration & Production, Houston, TX, USA*

ABSTRACT
Controlled-source electromagnetics (CSEM), is a geophysical electromagnetic method used to detect hydrocarbon reservoirs in deep-ocean settings. CSEM is used as a derisking tool by the industry but it is limited by the size of the target, low-spatial resolution, and depth of the reservoir. Synthetic aperture, a technique that increases the size of the source by combining multiple individual sources, has been applied to CSEM fields to increase the detectability of hydrocarbon reservoirs. We apply synthetic aperture to 3D diffusive fields with a 2D source distribution to evaluate the benefits of the technique. We also implement beamforming to change the direction of propagation of the field which allows us to increase the illumination of a specific area of the diffusive field. Traditional visualization techniques for electromagnetic fields, that display amplitude and phase, are useful to understand the strength of the electromagnetic field but they do not show direction. We introduce a new visualization technique utilizing the gradient and phase to view the direction of the diffusive fields. The phase-binned gradient allows a frequency-domain field to appear to propagate through time. Synthetic aperture, beamforming, and phase-binned gradient visualization are all techniques that will increase the amount of information gained from CSEM survey data.

Key words: synthetic aperture, CSEM

1 INTRODUCTION

Diffusive fields are used in many different areas of science; in this paper we use diffusive fields as an approximation for electromagnetic fields to demonstrate the benefits of synthetic aperture, beamforming, and viewing fields with a visualization technique involving the phase and gradient. This work is motivated by the use of diffusive fields used in controlled-source electromagnetics (CSEM), a geophysical electromagnetic method for detecting hydrocarbon reservoirs in deep-ocean settings. In CSEM, a horizontal antenna is towed just above the seafloor, where seafloor electromagnetic receivers are placed. CSEM was first developed in academia by Charles Cox in the 1970s and since then CSEM has been adopted by the industry and is used for derisking in the exploration of hydrocarbon reservoirs (Constable and Srnka, 2007; Edwards, 2005; Constable, 2010). The electromagnetic field in CSEM is predominantly diffusive because the source is low frequency and the signal propagates in a conducting medium. CSEM has some limitations that keep it from competing with other geophysical methods such as seismic. The size of the hydrocarbon reservoir must be large enough compared to the depth of burial to be detected and the signal that propagates through the reservoir is weak when compared to the rest of the signal (Constable and Srnka, 2007; Fan et al., 2010). Also, CSEM has low spatial resolution compared to seismic methods (Constable, 2010). These drawbacks prompted an investigation into improving the signal received from the hydrocarbon reservoir through synthetic aperture, a method developed for radar and sonar that constructs a larger virtual source by using the interference of fields created by different sources (Barber, 1985; Bellettini and Pinto, 2002). Fan et al. (2010) demonstrated that the wave-based concept of synthetic aperture sources can also be applied to a diffusive field and that it can improve the detectability of reservoirs. The similarities in the frequency-domain expressions of diffusive and wave fields show that a diffusive field at a single

frequency does have a specific direction of propagation (Fan et al., 2010). Once synthetic aperture is applied, the field can be steered using beamforming, a technique used to create a directional transmission from a sensor array (see Haynes, 1998; Van Veen and Buckley, 1988). The basic principles of phase shifts and addition can be applied to a diffusive field to change the direction in which the energy moves. These create constructive and destructive interference between the energy propagating in the field which, with a CSEM field, can increase the illumination of the reservoir (Fan et al., 2012). Manipulating diffusive fields by using interference is not necessarily new; the interference of diffusive fields has been used previously in physics for a variety of applications (Yodh and Chance, 1995; Wang and Mandelis, 1999). Fan et al. (2010) were the first to apply both concepts of synthetic aperture and beamforming to CSEM fields with one line of sources. Fan et al. (2012) demonstrate the numerous advantages of synthetic aperture steering and focusing to CSEM fields with a single line of sources; the detectability for shallow and deep targets greatly improves with the use of synthetic aperture. We extend this work by expanding the technique to a 2D source distribution. In this paper, we introduce the concept of 3D synthetic aperture for diffusive fields, provide examples of steered diffusive fields, present a new visualization technique, and provide examples demonstrating the benefits viewing diffusive fields with a phase-binned gradient.

2 3D SYNTHETIC APERTURE AND BEAMFORMING

2.1 Mathematical Basis

Synthetic aperture was first applied to diffusive fields by Fan et al. (2010) with one line of sources. Before this new use, synthetic aperture was used for radar, sonar, medical imaging and other applications (Barber, 1985; Bellettini and Pinto, 2002; Jensen et al., 2006). One reason synthetic aperture, a wave-based concept, has not been previously applied to diffusive fields is that it was thought diffusive fields could not be steered because they have no direction of propagation (Mandelis, 2000). Fan et al. (2010) showed that the 3D scalar diffusion equation has a plane wave solution at a single frequency with a defined direction of propagation which allows the direction of the field to be manipulated by synthetic aperture. The 3D scalar homogeneous diffusion equation is an appropriate approximation of a CSEM field because at a low frequency and in conductive media, like the subsurface, CSEM fields are diffusive (Constable and Srnka, 2007). In the frequency domain, the 3D scalar diffusion equation in a homogeneous medium, under the Fourier convention $f(t) = \int F(\omega)e^{-i\omega t}d\omega$, is given by

$$D\nabla^2 G(\mathbf{r},\mathbf{s},\omega) + i\omega G(\mathbf{r},\mathbf{s},\omega) = -\delta(\mathbf{r}-\mathbf{s}), \quad (1)$$

where D is the diffusivity of the medium, δ is the Dirac-Delta function, ω is the angular frequency, and $G(\mathbf{r},\mathbf{s},\omega)$ is the Green's function at receiver position $\mathbf{r}$ and source location $\mathbf{s}$. For synthetic aperture, we start with a diffusive field created from one point-source. The field from a point-source is given by

$$G(\mathbf{r},\mathbf{s},\omega) = \frac{\mathbf{1}}{\mathbf{4\pi D} \mid \mathbf{r}-\mathbf{s} \mid}\mathbf{e}^{-\mathbf{ik}|\mathbf{r}-\mathbf{s}|}\mathbf{e}^{-\mathbf{k}|\mathbf{r}-\mathbf{s}|}, \quad (2)$$

(Mandelis, 2000) where $G(\mathbf{r},\mathbf{s},\omega)$ is the Green's function at receiver position$\mathbf{r}$ and source location $\mathbf{s}$, ω is the angular frequency, and D is the diffusion constant. The wave number is given by $k = \sqrt{\omega/(2D)}$. The field from a point-source is the building block for synthetic aperture with diffusive fields. Multiple point-source fields can be summed to create one large source; the interference of the different sources combines to create a synthetic aperture source with greater strength than an individual point-source. The equation for synthetic aperture is given by

$$S_A(\mathbf{r},\omega) = \iint\limits_{sources} e^{-A}e^{-i\Delta\Psi}G(\mathbf{r},\mathbf{s},\omega)d\mathbf{s}, \quad (3)$$

where, for the source $\mathbf{s}$, $\Delta\Psi$ is the phase shift and A is an energy compensation coefficient. A traditional CSEM survey tows a source in parallel lines over receivers placed on the seafloor (Constable and Srnka, 2007); in the following we assume that the sources are towed along parallel lines that are parallel to the x-axis. Then we assume, also, that the y-axis is aligned with the crossline direction. The field is steered by applying a phase shift, for either inline steering or crossline steering, and energy compensation terms defined below:

$$\Delta\Psi = k\hat{\mathbf{n}}\boldsymbol{\Delta}\mathbf{s} \quad (4)$$

$$\hat{\mathbf{n}} = \begin{pmatrix} \cos\varphi\sin\theta \\ \sin\varphi\sin\theta \\ \cos\theta \end{pmatrix} \quad (5)$$

$$A = \Delta\Psi. \quad (6)$$

The phase shift, for an individual source, is shown in equation 4. The shift is a function of the wavenumber, the steering angle $\hat{\mathbf{n}}$, and a distance Δs. Equation 5 defines the steering direction which is controlled by two angles, θ and φ. The dip of the direction of the steering angle, represented by θ, is measured with respect to the vertical. The other angle, φ, represents the azimuthal direction. For inline steering, $\varphi = 0^\circ$ and for crossline steering, $\varphi = 90^\circ$; these are the only directions for φ considered in this work because they offer the best steering for a traditional CSEM survey set-up. The quantity, $\Delta s = \mid \mathbf{s_n} - \mathbf{s_1} \mid$ is the distance between an individual source, $\mathbf{s_n}$, and the source defined to be at the

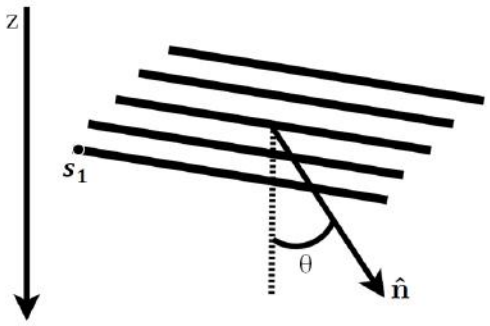

Figure 1. The design of a traditional CSEM survey. The individual source, $\mathbf{s_1}$, is defined to be located at the origin. The steering angle, $\hat{\mathbf{n}}$, is a function of θ, the dip and φ which is either 0° or 90° to steer in the inline or crossline directions, respectively.

bottom left corner of the survey footprint, $\mathbf{s_1}$. In general, the phase shift is defined as $\Delta\Psi = k(n_x\Delta s_x + n_y\Delta s_y)$. For inline steering, the phase shift equation simplifies to $\Delta\Psi = k\sin\theta\Delta s_x$ and for crossline steering, the equation simplifies to $\Delta\Psi = k\sin\theta\Delta s_y$ where Δs_x is the distance between the two sources in the x-direction and Δs_y is the distance between the sources in the y-direction. Figure 1 demonstrates a traditional CSEM survey design with the steering angle and s_1 labeled. To achieve the final steered field, $G(r, s, \omega)$ is summed over all sources in each individual line and, then, summed over all lines, as shown in equation 3. The exponential weighting, shown in equation 6, is just one way to create the interference needed to steer diffusive fields (Fan et al., 2012). For a homogeneous medium, the phase shift and energy compensation term are set to be equal because the decay of the field is proportional to the phase shift, and the attenuation coefficient in equation 2 is equal to the wave number (Fan et al., 2011). For a CSEM field, the energy compensation term accounts for the diffusive loss, decreases the background field to create a window to view the secondary field and equalizes the interfering fields to create destructive interference (Fan et al., 2011, 2012). We demonstrate the benefits of synthetic aperture and beamforming with numerical examples.

2.2 Numerical Examples

For all of the models shown in the next examples, the model volume is 20km×20km×4km to approximate the depth, width, and length of a traditional CSEM survey. We use parallel lines of sources which are the standard survey set-up in industry; in these examples, the 2D source distribution used is constructed from five 5km long tow lines that each contain 50 individual point-sources. The lines are spaced 2km apart which is a common spacing for receivers in the crossline direction. Diffusive fields are difficult to visualize with a linear scale because the field varies over many orders of magnitude. Therefore we use the transformation defined by Fan et al. (2010) to view the field's amplitude and sign with a logarithm to account for the rapid decay of the field. The transform is shown below:

$$I_G = m * Im(S_A) \tag{7}$$

$$Z = sgn(I_G)log_{10} \mid I_G \mid . \tag{8}$$

The factor m, in equation 7, is a constant scaling factor which sets the smallest amplitude of $\mid S_A \mid$ equal to 10^0. The dimensionless Z field displays the log of I_G with a minus sign when I_G is negative. The diffusive field from a point-source is shown in Figure 2. All the fields are created at a frequency of 0.25 Hz and a diffusivity $D = 2.4 \times 10^5$ m^2/s which is the approximate diffusivity of an electromagnetic wave in seawater (Fan et al., 2010). Figure 2 demonstrates how the field excited by a single point source diffuses through a 3D volume; the strength of the field decreases with increasing depth. We then apply synthetic aperture to the 2D source distribution in the inline and crossline directions. The unsteered field depicted in Figure 3 has five synthetic aperture sources each 5 km long. The sources in the five lines are summed, without any phase shifts and amplitude factors applied, in the x- and y-directions to produce a larger, longer source.

In CSEM the longest source dipole is around 300 meters (Constable, 2010); with synthetic aperture, we can create a much longer source without requiring a boat to tow the extra-long source. Beamforming is applied to the field to change the direction of the energy. For inline steering, individual sources in each of the five lines are multiplied by a phase shift and an energy compensation term and then the sources are summed. The inline direction has more sources to use because the source is towed in the x-direction with samples taken every 100 meters. Figure 4 demonstrates how steering caused the field to be asymmetric towards negative x-values. The diffusive field is steered in the crossline direction much the same way as in the inline direction, but a different phase shift is applied to each synthetic aperture source with all the individual sources on one line multiplied by the same phase shift. As shown in figure 5, this produces an asymmetric movement of the strength of the field in the negative y-direction. It is promising that even with five lines spaced 2km apart, we can achieve a marked crossline steering of the field; the maximum of the field has been shifted to the right away from the centerline of the survey ($y = 0$km). This leads us to believe that once applied to CSEM, crossline steering may direct the field toward a target. Inline and crossline steering can be combined to create a field that has energy shifted in the x- and y-directions (Figure 6). The combined steering creates a field that is asymmetric with respect to both axes, concentrating the energy in on area.

Applying synthetic aperture to diffusive fields

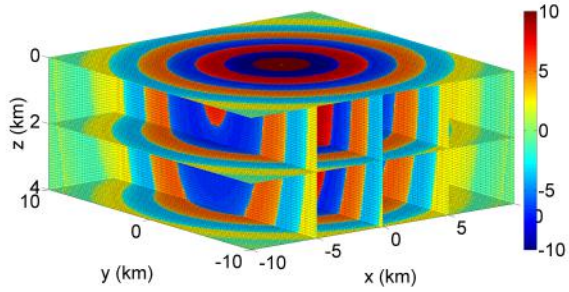

Figure 2. The point-source 3D scalar diffusive field log-transformed with the source at (0,0,0).

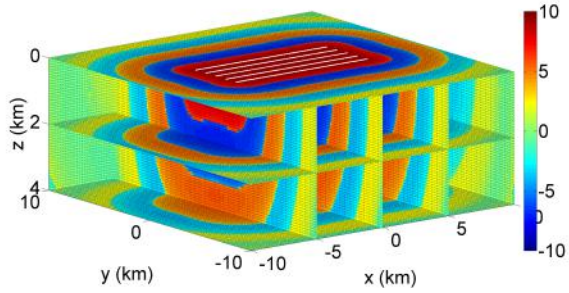

Figure 3. The unsteered 3D scalar diffusive field log-transformed.

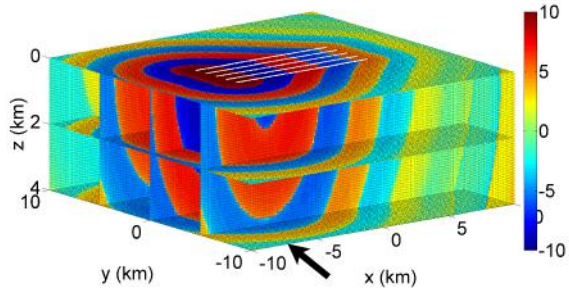

Figure 4. The 3D scalar diffusive field log-transformed and steered at a 45° angle in the inline direction. The arrow shows the shift in the x-direction of the energy from the origin; without steering the maximum energy would be located at the center of the source lines (x= 0km).

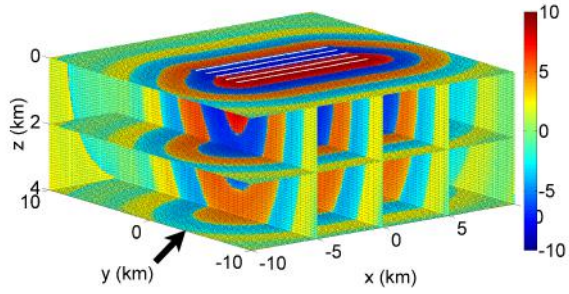

Figure 5. The 3D scalar diffusive field log-transformed and steered at a 45° angle in the crossline direction. The arrow shows the shift in the energy from the centerline of the survey (y= 0km). The shift is less than in Figure 4 because fewer sources are used.

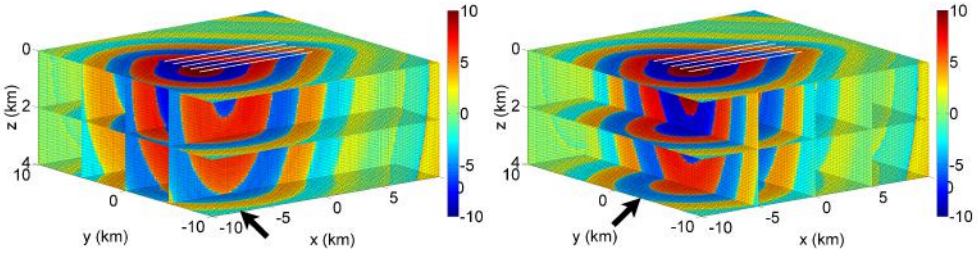

Figure 6. The 3D scalar diffusive field log-transformed and steered at a 45° angle in the inline and crossline directions. The arrows demonstrate the shift in the energy in the x- and y- directions.

demonstrates the possibilities of using 3D synthetic aperture on real electromagnetic fields acquired from CSEM surveys. The inline and crossline steering of diffusive fields shows how the maximum can be shifted to a new area which allows that area to be illuminated than without steering. The log-transform is a useful tool to view diffusive fields but it has some drawbacks. The only information communicated is the sign and normalized amplitude of the field. There is no information about the direction of the field or a sense of how it propagates in 3D space. We developed a new way to visualize the fields that shows the direction and propagation of the fields in the frequency-domain.

3 3D VISUALIZATION

3.1 Mathematical Basis

The most common way to visualize electric and magnetic field is through magnitude and phase plots but these lack the capability to show the direction the field is traveling (Constable, 2010). Additionally, the log-transformation employed in the previous figures only shows the sign and normalized amplitude of the field, but we need to visualize the direction of the field to identify the enhancement of the upgoing field from synthetic aperture and beamforming because the most important information from a CSEM survey is the electromagnetic signal that propagates down, through the reservoir, and then returns to the seafloor to be recorded by a receiver. This signal is difficult to identify because it is much weaker compared to the background field. The Poynting vector measures the direction in which the energy flux of the electromagnetic field is traveling; it is an effective way to examine how an electromagnetic field propagates (Fan et al., 2012). The energy flux density of the electromagnetic field is given by (Griffiths, 2008)

$$\mathbf{S} \equiv \frac{1}{\mu_o}\mathbf{E} \times \mathbf{B}, \tag{9}$$

where μ_o is the permeability of free space, $\mathbf{E}$, is the electric field, and $\mathbf{B}$ is the magnetic field. The diffusive field, an approximation of a diffusive electric field, we use is a scalar field and therefore the Poynting vector cannot be used. The gradient of a scalar field is, however, similar to the Poynting vector for an electromagnetic field: the Poynting vector is the energy flux density of the electromagnetic field which is similar to the heat flux density used in thermodynamics. The heat flux density is found by taking the gradient of temperature which makes the gradient a useful measure of the energy flux for scalar diffusive fields (Schroeder, 1999). The gradient of a diffusive field is complex and only the real part is used to display the gradient, normalized to make the direction apparent. In addition to visualizing the direction of the field, it is useful to know the direction of the field in relation to the time over which the field has propagated; the use of the phase of the field in conjunction with the gradient allows a frequency-domain field to appear to propagate through time. A simple example demonstrates this concept. Consider a point-source field, e^{ikr} where k is the wavenumber and r is the distance from the source to another location in space. In that case, the phase is, then, equal to kr which smoothly increases with respect to r. A small phase corresponds to a location close to the source and a large phase corresponds to a location farther away from the source. Thus, when the phase is binned by multiplies of π the frequency-domain diffusive field appears to propagate outward in space the same way it propagates through time. The phase must not contain phase-jumps for use in our visualization method. To make the phase of the field increase smoothly, we use phase-unwrapping in 3D which corrects the phase-jumps of 2π that occur in the field. Phase unwrapping is applied in many fields including radar, medical, and geophysics; 3D phase unwrapping is an ongoing field of research (Itoh, 1982; Wang et al., 2011; Parkhurst et al., 2011; Shanker and Zebker, 2010). Phase unwrapping is simple for our noiseless scalar diffusive fields; we unwrap the phase one dimension at a time to construct a smoothly increasing phase. Phase jumps determined to be larger than the tolerance value π are reduced by adding or subtracting 2π to until the jump is less than the tolerance value. Once the phase is unwrapped, we add a constant to the phase field to make the source phase equal to zero. Only the relative

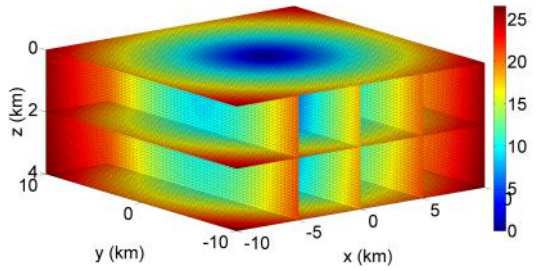

Figure 7. The unwrapped phase of a scalar diffusive field from a point-source located at (0,0,0). The colorbar displays radians.

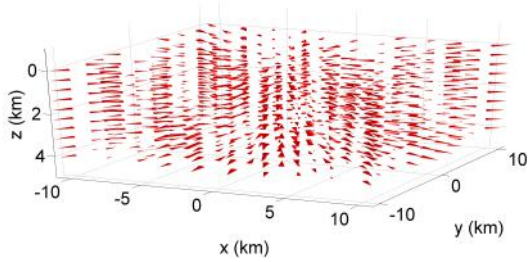

Figure 8. The normalized gradient of a scalar diffusive field from a point-source location at (0,0,0).

phase is needed to view a scalar diffusive field with this method. The source is time-varying with a period of four seconds, which creates a change in the direction of the field; to show only one type of direction on the image, the phase is binned by multiples of π. The gradient that corresponds to each phase bin is shown consecutively; as the phase increases the gradient is displayed at an increasing distance from the source.

3.2 Numerical Examples

As in the previous section, the volume of the diffusive field is 20km×20km×4km to represent a CSEM survey area. We first demonstrate the phase-binned gradient visualization technique with a simple point-source before applying the method to a field with a synthetic aperture source. The phase and gradient are shown in Figures 7 and 8 to compare with the 3D phase-binned gradient in Figure 9.

The temporal evolution of the field cannot be viewed with the gradient or the phase. The advantage of the phase-binned gradient is that it displays the direction of the energy from the origin outward to the edges of the model as a function of increasing phase. The direction of the field is displayed for different phase bins; a smaller phase corresponds to parts of the field closer to the source and a larger phase corresponds to parts of the field farther away from the source. This type of visualization becomes more useful when examining a field

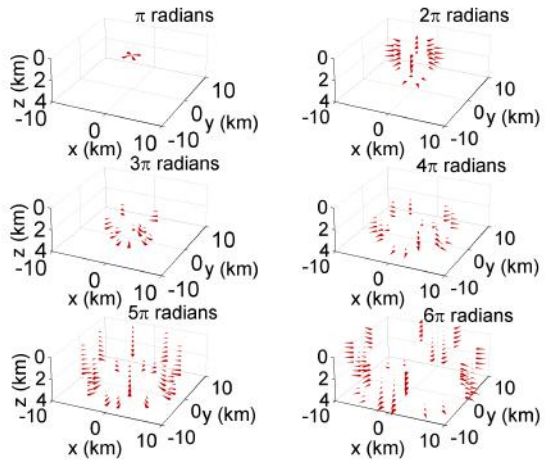

Figure 9. The phase-binned gradient of a scalar diffusive field from a point-source located at (0,0,0). The change in direction occurs from the time-harmonic point-source.

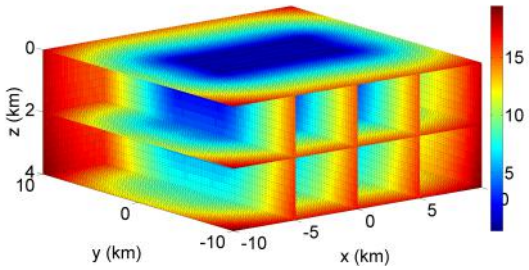

Figure 10. The unwrapped phase of a scalar diffusive field with five lines of synthetic aperture sources. The colorbar displays radians.

with synthetic aperture and steering which are more complex than the point-source example. Figures 10 and 11 display the unwrapped phase and gradient, respectively, of a scalar diffusive field with five 5km synthetic aperture sources.

The phase of the unsteered diffusive field (Figure

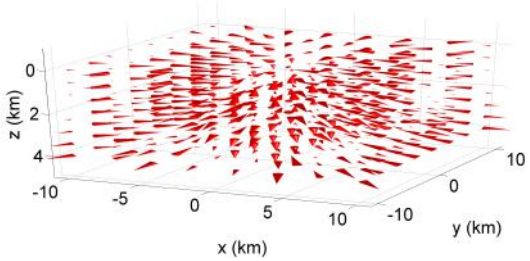

Figure 11. The normalized gradient of a scalar diffusive field with five synthetic aperture sources.

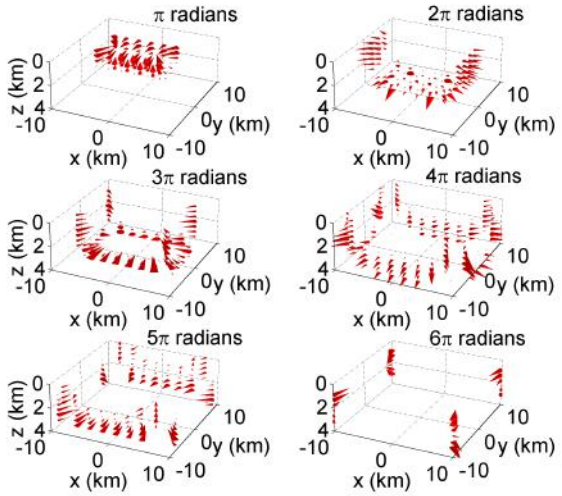

Figure 12. The phase-binned gradient of a scalar diffusive field with five unsteered synthetic aperture sources. The movement of the energy is symmetric about both the x and y directions.

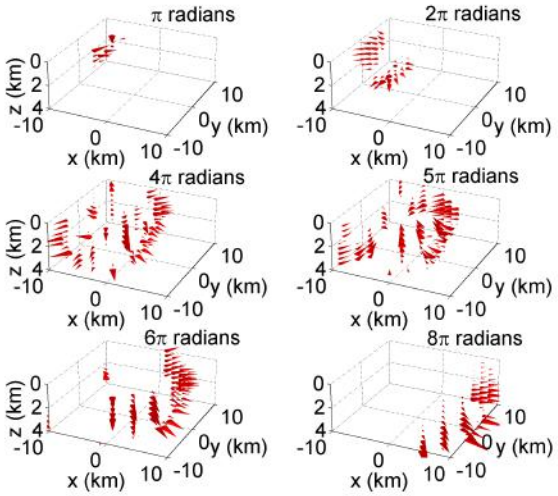

Figure 13. The phase-binned gradient of a scalar diffusive field with five synthetic aperture sources steered in the inline direction at a 45°. The energy is moving asymmetrically in the x-direction unlike the symmetric movement of the unsteered field.

10) created from synthetic aperture sources displays the change to a 2D source distribution when compared with the phase of the point-source (Figure 7). However, it does not show the change in the direction as a result of the application of synthetic aperture because no steering is applied to this example. The gradient of the unsteered diffusive field, Figure 11, does display the direction of the field but it is difficult to see the differences between the unsteered synthetic aperture source and the point-source gradient, shown in Figure 8. The phase-binned gradient of the unsteered diffusive field allows the differences to be highlighted. Figure 12, in comparison to Figure 9, demonstrates the effect of synthetic aperture through the broadening of the pattern of arrows depicted in each phase, a result of the 2D distribution of the synthetic aperture source.

The inline and crossline phase-binned gradient plots (Figures 13 and 14) demonstrate how the direction of energy propagation changes with the use of beamforming. The inline field, shown in Figure 13, is steered at a 45° angle in the inline direction which causes constructive interference to occur at large x values compared to the unsteered field in Figure 12, which has the same amount of energy at all values of x. The interference is difficult to view with the log-transform, as previously shown in Figure 4, because the amplitude of the energy is small in the area 45° from the x-axis. The crossline field is steered at 45° which is visible in the lower right panels of Figure 14 as a preferential propagation in the crossline direction (large values of y). Rather than staying symmetric about the y-axis, the crossline steering causes the interference to occur at large y values in late phases. As with the inline field, this is difficult

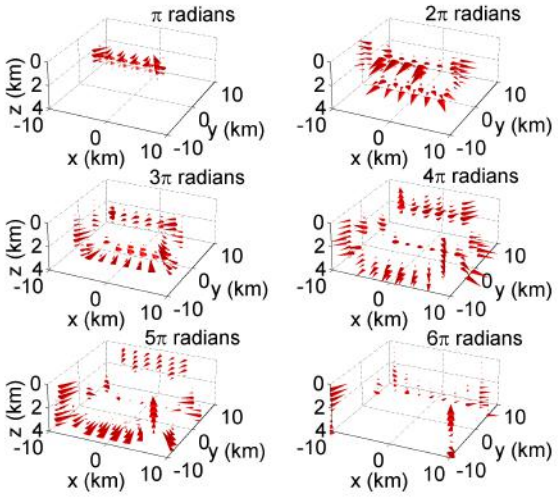

Figure 14. The phase-binned gradient of a scalar diffusive field with five synthetic aperture sources steered in the crossline direction at 45°. The energy is moving asymmetically in the negative y-direction in contrast to the symmetric movement of the unsteered field.

to visualize without the phase-binned display of the direction of propagation. The combination of inline and crossline steering produces a diffusive field with energy in one area of the model. In Figure 15, the concentration of energy to large x and y values is displayed in the later phases of the field. Without the phase-binned gradient technique the change in the direction due to beamform-

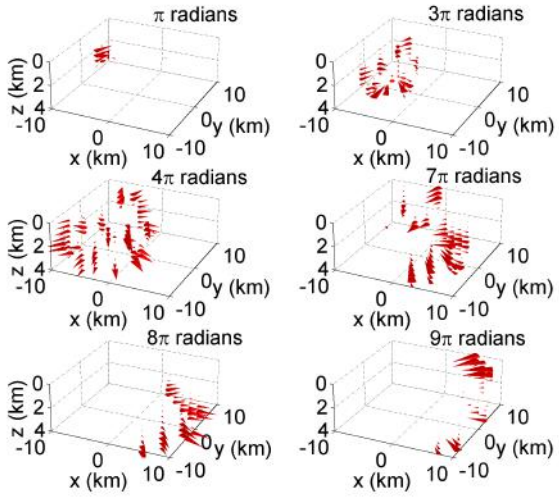

Figure 15. The phase-binned gradient of a scalar diffusive field steered in the inline and crossline directions at 45°. The combined inline and crossline steering produces a field whose energy moves out asymmetrically in both the x- and y-directions.

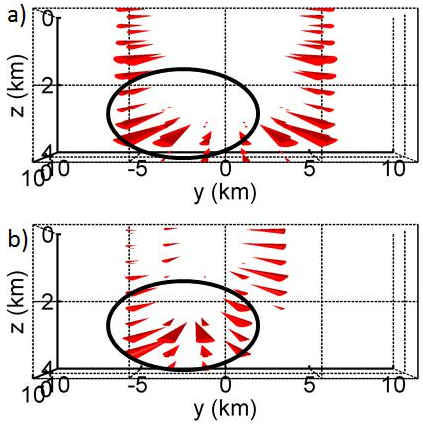

Figure 16. The y-z view of the unsteered diffusive field, panel a), and the combined inline and crossline steered diffusive field, panel b), at a phase of 3π. The oval highlights the change in the direction of the field caused by steering.

ing is nearly impossible to visualize, especially with in a 3D volume. Figure 16 depicts an y-z view of the unsteered diffusive field gradient and the combined inline and crossline steered diffusive field gradient. The oval shape highlights the change in the direction of the field cause by steering. The unsteered field, panel a) of Figure 16, has mostly horizontal arrows. When steering is performed, panel b) of Figure 16, the arrows change to have an increased upward direction. CSEM measurements are effective for detecting reservoirs when the field propagates in the near vertical directions. Figure 16 demonstrates that with a diffusive field steering can modify the direction the energy propagates.

The differences in the direction of the diffusive fields can be used to determine if the synthetic aperture is steered optimally for a specific example. For CSEM fields, where the Poynting vectors are used instead of the gradient the goal is to increase the amount of upgoing energy that carries information about the reservoir. This visualization method will identify how the field propagates and how to optimize the beamforming parameters.

4 DISCUSSION AND CONCLUSIONS

The synthetic aperture technique offers a way to address some of the limitations of CSEM without requiring any changes in acquisition. Applying the technique to diffusive fields with 2D source distributions demonstrates the possibilities the technique has to increase the detectability of hydrocarbon reservoirs with CSEM fields. Steering the fields in both the inline and crossline directions causes the strength of the field to move to a localized area. Research is ongoing to apply this technique to synthetic CSEM fields to quantify the benefits of steering with a 2D source. The new visualization technique we introduce demonstrates how a frequency-domain field can appear to propagate as a function of increasing phase. The combined phase and gradient (or Poynting vector) provide a way to visualize how the steering modifies the upgoing field so that amount of information about the target is maximized. This is an improvement over other visualization methods that only show the amplitude or sign of the field. The implementation of these techniques increases the amount of information gleaned from data acquired from the CSEM survey, making CSEM a more valuable tool for industry. The next step is to apply the methods to electromagnetic fields with reservoirs. We will investigate what type of acquisition geometry maximizes the benefits of steering with synthetic aperture and how to optimize the steering.

ACKNOWLEDGMENTS

We are grateful for the financial support from the Shell Gamechanger Program of Shell Research, and thank Shell Research for the permission to publish this work.

References

Barber, B. C., 1985, Theory of digital imaging from orbital synthetic-aperture radar: International Journal of Remote Sensing, **6**, 1009–1057.

Bellettini, A., and M. A. Pinto, 2002, Theoretical accuracy of synthetic aperture sonar micronavigation using a displaced Phase-Center antenna: IEEE Journal of Oceanic Engineering, **27**, 780–789.

Constable, S., 2010, Ten years of marine CSEM for hydrocarbon exploration: Geophysics, **75**, 75A67–75A81.

Constable, S., and L. J. Srnka, 2007, An introduction to marine controlled-source electromagnetic methods for hydrocarbon exploration: Geophysics, **72**, WA3–WA12.

Edwards, N., 2005, Marine controlled source electromagnetics: Principles, methodologies, future commercial applications: Surveys in Geophysics, **26**, 675–700.

Fan, Y., R. Snieder, E. Slob, J. Hunziker, and J. Singer, 2011, Steering and focusing diffusive fields using synthetic aperture: Europhys. Lett., **95**, 34006.

Fan, Y., R. Snieder, E. Slob, J. Hunziker, J. Singer, J. Sheiman, and M. Rosenquist, 2010, Synthetic aperture controlled source electromagnetics: Geophysical Research Letters, **37**, L13305.

———, 2012, Increasing the sensitivity of controlled-source electromagnetics with synthetic aperture: Geophysics, **77**, E135.

Griffiths, D. J., 2008, Introduction to electrodynamics: Pearson.

Haynes, T., 1998, Beamforming: A primer: www.spectrumsignal.com.

Itoh, K., 1982, Analysis of the phase unwrapping algorithm: Applied Optics, **21**, 2470.

Jensen, J. A., S. I. Nikolov, K. L. Gammelmark, and M. H. Pedersen, 2006, Synthetic aperture ultrasound imaging: Ultrasonics, **44**, e5–e15.

Mandelis, A., 2000, Diffusion waves and their uses: Physics Today, **53, 8**, 29–34.

Parkhurst, J., G. Price, P. Sharrock, and C. Moore, 2011, Phase unwrapping algorithms for use in a true real-time optical body sensor system for use during radiotherapy: Applied Optics, **50**, 6430–6439.

Schroeder, D. V., 1999, An introduction to thermal physics: Addison Wesley.

Shanker, A. P., and H. Zebker, 2010, Edgelist phase unwrapping algorithm for time series InSAR analysis: Journal of the Optical Society of America A, **27**, 605.

Van Veen, B., and K. Buckley, 1988, Beamforming: a versatile approach to spatial filtering: IEEE ASSP Magazine, **5**, 4–24.

Wang, C., and A. Mandelis, 1999, Purely thermal-wave photopyroelectric interferometry: Journal of Applied Physics, **85**, 8366–8377.

Wang, H., J. B. Weaver, I. I. Perreard, M. M. Doyley, and K. D. Paulsen, 2011, A three-dimensional quality-guided phase unwrapping method for MR elastography: Physics in Medicine and Biology, **56**, 3935–3952.

Yodh, A., and B. Chance, 1995, Spectroscopy and imaging with diffusing light: Physics Today, **48, 3**, 34–40.